

# Thermal and electrical properties of composites based on (3-mercaptopropyl) trimethoxysilane- and Cu-coated carbon fiber and silicone rubber

Xiong-wei Zhao<sup>1</sup> · Chong-guang Zang<sup>1</sup> · Qing-kun Ma<sup>2</sup> · Yu-quan Wen<sup>1</sup> · Qing-jie Jiao<sup>1</sup>

Received: 24 October 2015 / Accepted: 5 January 2016 / Published online: 12 January 2016  
© Springer Science+Business Media New York 2016

**Abstract** In this paper, (3-mercaptopropyl)trimethoxysilane (MPTS)- and copper-coated carbon fiber (M–Cu–CF) was obtained by electroless plating method. The M–Cu–CF was evaluated by FTIR, XRD, TGA, and SEM. It was found that the MPTS and Cu were coated on the fiber surface successfully. The M–Cu–CF was utilized as a conductive filler in silicone rubber (SR) for thermal and electrical conductivity applications and exhibited good dispersion and compatibility with the matrix. The effect of M–Cu–CF content on the thermal conductivity and volume resistivity of silicone rubber composites was investigated. The results showed that the thermal conductivity of the M–Cu–CF/SR composites reached  $1.99 \text{ W (m K)}^{-1}$  with only 4.0 wt% filler loading, approximately 2.10 times higher than that of raw-CF/SR composites at the same loading. And with the increase of M–Cu–CF loading, the least volume resistivity of M–Cu–CF/SR composites was  $3.5 \times 10^3 \Omega \text{ cm}$ .

## Introduction

It is widely known that silicone rubber (SR) is utilized in a large variety of applications thanks to its good chemical resistance, low density, weather resistance, and so on [1–5]. However, the poor thermal and electrical conductivities of

SR have tremendously hindered its further utilization, particularly for the sealing of electronic devices. It is difficult for the potted device to dissipate the excess heat, finally resulting in damage or a reduced lifetime of the device. In addition, for some sensitive components, the accumulated static electricity can largely reduce the sensitivity of the device. To ease this situation, researchers have sought out a common method through preparing conductive filler/SR composites [6–10]. As examples, Chiu et al. fabricated silicon-based ceramics and aluminum nitride (Si/AlN), and researched the thermal conductivity of the composites [11]. Ismail et al. investigated the effect of TiB<sub>2</sub> nanopowder and carbon black (CB) on the electrical conductivity of silicone rubber/CB/TiB<sub>2</sub> composites [12]. Mu et al. studied the thermal conductivity of silicone rubber filled with ZnO in a wide volume range, and discussed the effect of formed conductive particle chains on the thermal conductivity of composites [13]. Although the thermal and electrical conductivities of silicone rubber composites have been enhanced by filling the conductive fillers, the results, a moderate growth, are not satisfactory. Moreover, to obtain appropriate thermal and electrical conductive properties, the viscosity of the silicone rubber composites ahead of curing becomes very high, which does not contribute to the applications.

To solve this problem, a highly efficient thermal and electrical conductive filler should be synthesized. Traditional conductive fillers include carbon-based materials and metal powder materials. Among them, carbon fibers (CFs), one of the most important and advanced carbon-based materials, are widely used to reinforce polymer composites due to its high strength and conductivity and low density [14–16]. And copper is used as a highly efficient conductive filler in recent years [17, 18]. With the development of metallization technology, copper-plated carbon fibers will

✉ Chong-guang Zang  
zangchongguang@bit.edu.cn

<sup>1</sup> State Key Laboratory of Explosive Science and Technology, Beijing Institute of Technology, Beijing 100081, People's Republic of China

<sup>2</sup> Research Center of Yuxi Industries Group, Norinco Group, Nanyang 473000, People's Republic of China

share advantages of both carbon fibers and copper, possessing light weight and high thermal and electrical conductive properties.

In the present work, copper-coated carbon fiber (Cu-CF) was prepared by electroless plating method. And the MPTS was coated on the surface of Cu-CF to improve the compatibility and interaction with the matrix. M-Cu-CF/silicone rubber was obtained, and the effect of M-Cu-CF content on the thermal and electrical conductive properties of the silicone rubber composites was investigated.

## Materials and methods

### Materials

The polydimethylvinylsiloxane (PDVS) and polymethylhydrosiloxane (PMHS) were supplied by Shangdong Dayi Chemical Co., Ltd, China. The vinyl content of PDVS is 0.5 mol%, and the hydrogen content of PMHS is 0.3 mol%. A platinum catalyst and an inhibitor were synthesized in our laboratory. The carbon fibers (resistivity =  $1.6 \times 10^{-3} \Omega \text{ cm}$ , diameter = 6.5  $\mu\text{m}$ , length = 0.5–1 mm) were purchased from Liaoning Anke Carbon Fiber Co., Ltd, China. The MPTS was produced by Aladdin Industrial Corporation, China. Benzotriazole was purchased from Tianjin Guangfu Fine Chemical Research Institute, China. Sodium dodecyl sulfate and zinc powder were supplied by Tianjin Fuchen Chemical Reagents Factory, China. Copper sulfate pentahydrate ( $\text{CuSO}_4 \cdot 5\text{H}_2\text{O}$ ), tin(II) chloride dehydrate ( $\text{SnCl}_2$ ), silver nitrate ( $\text{AgNO}_3$ ),  $\text{HNO}_3$  (69 %, nitric acid),  $\text{HCl}$  (36 %, hydrochloric acid), ethanol, acetone, and toluene were received from Beijing Chemical Works, China.

### Preparation of copper-coated CF

Before coating copper on the CF surface, the CF was pretreated to remove the epoxy resin layer. The CF was placed into a muffle oven at 400 °C for 1 h, then washed with acetone and dried in a vacuum oven. To oxidize the CF surface (O-CF), the dried CF was immersed into 69 %  $\text{HNO}_3$  at 60 °C for 4 h, then washed with deionized water and dried for further use [16]. 5.0 g O-CF was added into 300 mL aqueous solution consisting of  $\text{HCl}$  (20 mL  $\text{L}^{-1}$ ) and  $\text{SnCl}_2$  (20.0 g  $\text{L}^{-1}$ ) at 45 °C for 45 min with stirring. After filtering, washing, and drying, the O-CF was added into 300 mL  $\text{AgNO}_3$  (15 g  $\text{L}^{-1}$ ) solution at 35 °C for 1 h, then washed and dried to obtain activated CF (Ag-CF) [19–21]. The silver atoms, on the CF surface, can initiate the deposition of Cu on CF surface as a catalyst. The scheme of preparation procedure is shown in Fig. 1. For coating copper on the Ag-CF surface, a typical electroless

process was used [22]. 5.0 g Ag-CF was dispersed into 250 mL  $\text{CuSO}_4$  (10 g  $\text{L}^{-1}$ ) solution in a 500-mL beaker at room temperature for 30 min with stirring. Then 10 mL sodium dodecyl sulfate (10 g  $\text{L}^{-1}$ ) was added into the system. And the mixture was sonicated for 1 h to obtain single fibers. During the ultrasonication process, the mixture was agitated discontinuously to prevent the Ag-CF precipitation. After that, 10 mL benzotriazole (15 g  $\text{L}^{-1}$ ) was added into the mixture with stirring for 30 min to prevent the oxidation of the coated copper. Then 0.5 g Zn powder was mixed into the system. The coating reaction was conducted for about 1 h with warm agitation. Eventually, the mixture solution was poured into  $\text{HCl}$  (1 mol  $\text{L}^{-1}$ ) to remove the unreacted Zn powder, and then filtered, washed with deionized water repeatedly, and dried. The copper-coated Ag-CF was labeled Cu-CF.

### Preparation of M-Cu-CF

Ten grams of Cu-CF was dispersed in 200 mL ethanol with mechanical agitation for 10 min in a three-neck flask. Then 2.0 mL MPTS was added into the mixture. The MPTS monolayer was formed on the copper surface for 24 h at room temperature. After the MPTS monolayer formation, the mixture was filtered and washed with ethanol for 3–5 times to remove the unreacted MPTS molecules. Afterwards it was dried in a vacuum oven at 60 °C. The functionalized Cu-CF was obtained and labeled M-Cu-CF (as shown in Fig. 1).

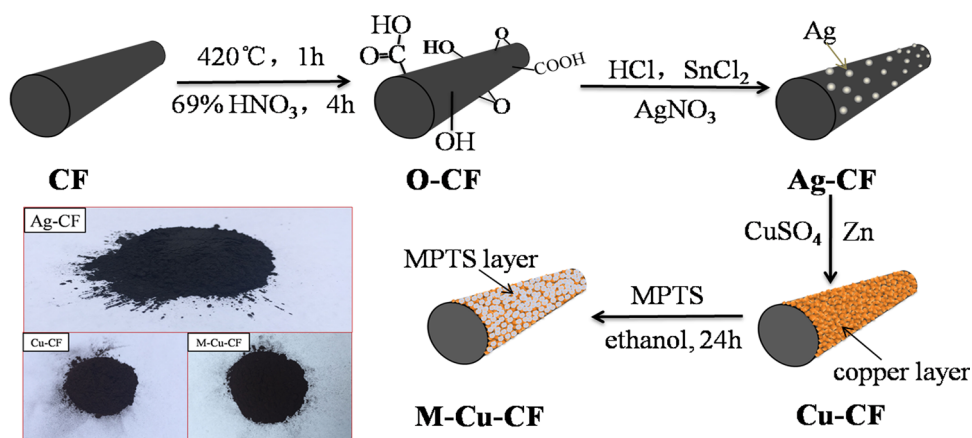
### Preparation of raw-CF/SR, Cu-CF/SR, and M-Cu-CF/SR composites

The various CFs were dispersed in toluene for 1 h by ultrasonication to achieve uniform dispersion. Then, the mixture solution was mixed with PDVS (3:1 weight ratio). After the PDVS was dissolved in toluene absolutely, the mixture was stirred at 70 °C until constant weight and a viscous CF/PDVS solution was obtained. Soon afterwards, the PMHS, platinum catalyst, and inhibitor were mixed with the CF/PDVS solution completely (PDVS: PMHS = 1: 2 weight ratio). After degassed to remove the air bubbles, the mixture was poured into a polytetrafluoroethylene mold with dimensions of 240 × 170 × 2 mm<sup>3</sup> and cured for 2 h at 80 °C. The composites containing different fillers and contents were prepared by the above-mentioned steps.

### Characterization

A Netzsch TG 209 F1 Iris thermogravimetric analyzer (TGA, Selb, Germany) was used to explore the thermal stabilities of materials from ambient temperature to 800 °C

**Fig. 1** Scheme of the procedure for preparation of M–Cu–CF



at a heating rate of  $10 \text{ K min}^{-1}$  under a nitrogen atmosphere. Fourier transform infrared (FTIR) spectra were obtained with an IFS 66 V/S FTIR spectrometer (Bruker, Germany). The different kinds of CFs were separately pressed into pellets with potassium bromide and then scanned from  $500$  to  $4000 \text{ cm}^{-1}$  at a resolution of  $4.0 \text{ cm}^{-1}$ . X-ray diffraction (XRD) was conducted by a Bruker D8 Advance X-ray diffractometer using  $\text{Cu}$  ( $K\alpha$ ) radiation ( $\lambda = 0.154 \text{ nm}$ ) with the step size  $0.014^\circ$  ranging from  $5^\circ$  to  $85^\circ$  at a speed of  $2^\circ \text{ min}^{-1}$ . The various CFs were separately pressed to form a plane for X-ray analysis. The morphological and elementary analysis of various CFs and composites was executed on a cold field emission scanning electron microscopy (SEM; S4800, Hitachi High-Technologies Corp.) equipped with an energy-dispersive X-ray spectroscopy (EDS) system. The fracture surfaces of the composites were coated with gold before scanning.

The thermal conductivities of composites were calculated with Eq. (1) in accordance with ASTM E1461:

$$\lambda = \alpha \times \rho \times c_p, \quad (1)$$

where  $\lambda$  is the thermal conductivity,  $\alpha$  is thermal diffusivity,  $\rho$  is the density, and  $c_p$  is the specific heat capacity. A Netzsch LFA 447 system (Selb, Germany) was used to test the thermal diffusivity with the temperature ranging from  $25$  to  $150^\circ\text{C}$ . The densities were calculated by Archimedeian method. The specific heat capacity was measured by a differential scanning calorimeter (DSC, Netzsch 200 F3 Maia, Selb, Germany). The temperature ranged from  $25$  to  $150^\circ\text{C}$  at a heating rate of  $10 \text{ K min}^{-1}$  under a nitrogen atmosphere.

An EST 991 electric and electrostatic shielding material volume resistivity measuring instrument was employed to measure the direct-current bulk electrical resistivity ( $\rho$ ;  $\Omega \text{ cm}$ ) of the composites by a four-contact scheme method. The  $\rho$  was calculated with Eq. (2):

$$\rho = \frac{Uwt}{Il}, \quad (2)$$

where  $U$  is the voltage,  $I$  is the current,  $w$  and  $t$  are the width and thickness of the specimens, respectively, and  $l$  is the distance between the testing metal electrodes. In our study, the values of the parameters  $w$ ,  $t$ , and  $l$  were  $10$ ,  $2$ , and  $20 \text{ mm}$ , respectively. Every specimen was measured three times at room temperature, and all samples were placed in a vacuum oven at  $60^\circ\text{C}$  for  $24 \text{ h}$  before testing.

## Results and discussion

### Characteristics of CF

The Fourier transform infrared (FTIR) spectra of (a) Ag-CF, (b) Cu-CF, and (c) M–Cu–CF are compared and shown in Fig. 2. A strong and broad peak at around  $3465 \text{ cm}^{-1}$  appears in all the samples that corresponds to the OH bonds from the C–OH groups [23]. The doublet at  $2922$  and  $2853 \text{ cm}^{-1}$  is attributed to the asymmetric (aCH<sub>2</sub>) and symmetric (sCH<sub>2</sub>) stretching modes of C–H bonds [24, 25].

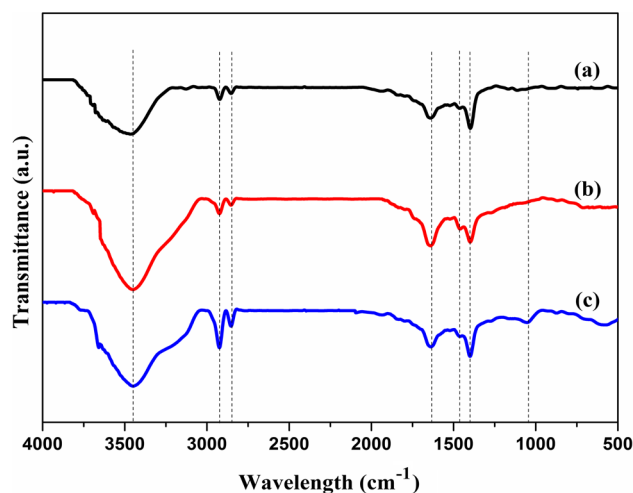


**Fig. 2** FTIR spectra of a Ag-CF, b Cu-CF, and c M–Cu–CF

The bands at 1639 and 1460  $\text{cm}^{-1}$  are assigned to the vibrations of C=C, and the band at 1384  $\text{cm}^{-1}$  corresponds to the O–H vibrations of C–OH groups [16]. In the spectrum of M–Cu–CF, a new band appears at 1035  $\text{cm}^{-1}$  corresponding to the stretching of Si–O–Si bond [25], which is attributed to the hydroxylation of MPTS in the solution. Moreover, the spectrum of M–Cu–CF exhibits a strong absorption at 2922 and 2853  $\text{cm}^{-1}$  compared to those of Ag–CF and Cu–CF, further demonstrating the formation of MPTS layer on the Cu–CF surface. Therefore, it is reasonable to deduce that the MPTS experiences hydrolysis and dehydration. Besides, the absence of the stretching of C–S or S–H bonds in the spectra may be ascribed to the formation of Cu–S between MPTS and Cu–CF.

Figure 3 exhibits the X-ray diffraction pattern of raw-CF, Cu–CF, and M–Cu–CF. The XRD pattern of raw-CF shows a broadened feature ranging from 18° to 32°, corresponding to the characteristic peak of the C (002) plane. And the peak at around 44.5° can be attributed to the C (10) plane [26]. After coating copper, the Cu–CF displays a decrescent C (002) peak and three new characteristic reflection peaks of (111), (200), and (220) appear on the diffraction pattern, indicating a typical crystal structure for Cu layer [27]. Moreover, there is no characteristic peak of CuO or Cu<sub>2</sub>O on the diffraction pattern, which means that the Cu layer is not oxidized. For M–Cu–CF, the XRD pattern has a similar tendency with the Cu–CF except a new broadening peak ranging from 7.5° to 15.4°, which is attributed to the amorphous nature of MPTS. This result confirms the formation of MPTS layer on the surface of Cu–CF, which is consistent with the consequence of FTIR previously.

Distinct materials exhibit different thermal stability and thermal decomposition behaviors [28]. Figure 4 shows the

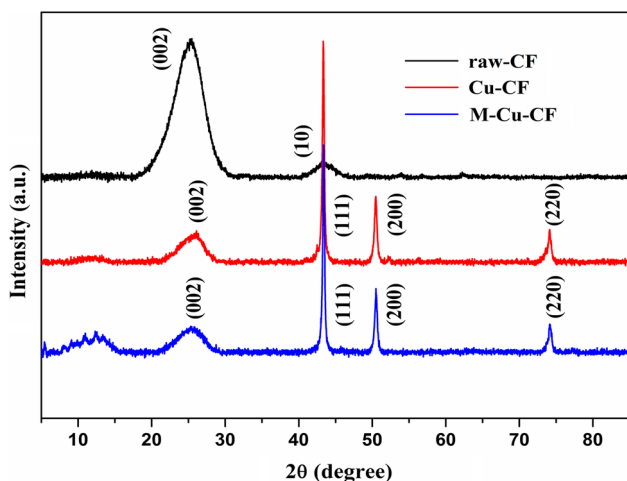


**Fig. 3** X-ray diffractograms of raw-CF, Cu–CF, and M–Cu–CF

TGA curves of the raw-CF, Ag–CF, Cu–CF, and M–Cu–CF. As observed from the curves, the raw-CF hardly decomposes until the temperature increases up to 800 °C, presenting high thermal stability [16, 29]. The slight weight loss is likely attributed to the amorphous carbon, volatile carbonaceous impurities, and the epoxy on the raw-CF surface. After oxidation, owing to the decomposition of some unstable oxygen-containing groups, Ag–CF displays a 2.66 wt% more weight loss than raw-CF. Compared with Ag–CF, Cu–CF exhibits nearly the same thermal behavior, since no unstable element is brought in the system. For M–Cu–CF, a 4.04 wt% more weight loss than Cu–CF is observed, which proves the formation of MPTS layer. Moreover, the TGA spectra of M–Cu–CF can be divided into two steps. From the beginning to 260 °C, the weight loss mainly results from the degradation of oxygen functionalities on the fiber surface. The second stage, from 260 to 480 °C, the weight loss is due to the decomposition of MPTS, further demonstrating the existence of MPTS layer on the surface of Cu–CF.

### Morphological analysis

Typical scanning electron micrograph (SEM) images of the fibers are shown in Fig. 5. It can be seen from Fig. 5a that the surface of the raw-CF is smooth and adheres to some epoxy. Although some stripe ravines can be discovered on the raw-CF (Fig. 5b), the existence of epoxy layer makes it impossible for the catalyst ions to deposit on the surface. After oxidation treatments, the Ag–CF surface becomes pure and the stripe-shaped ravines become obvious, which is indispensable for the adsorption of catalyst ions (Fig. 5c, d) [30]. The micrographs in Fig. 5e, f show the lower and higher magnification images of Cu–CF, respectively. It is revealed that the fibers are packed by the copper

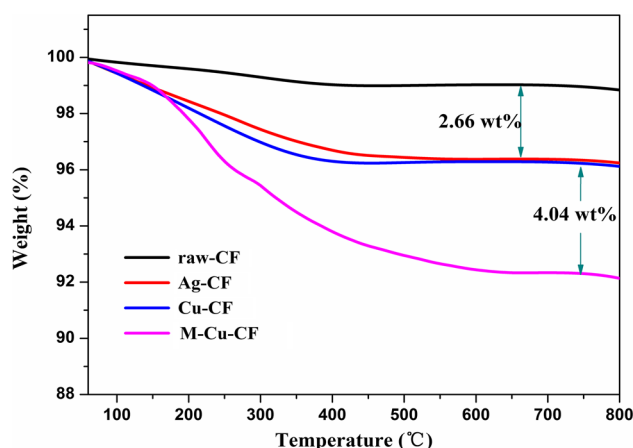


**Fig. 4** TGA curves of different types of carbon fibers: raw-CF, Ag–CF, Cu–CF, and M–Cu–CF

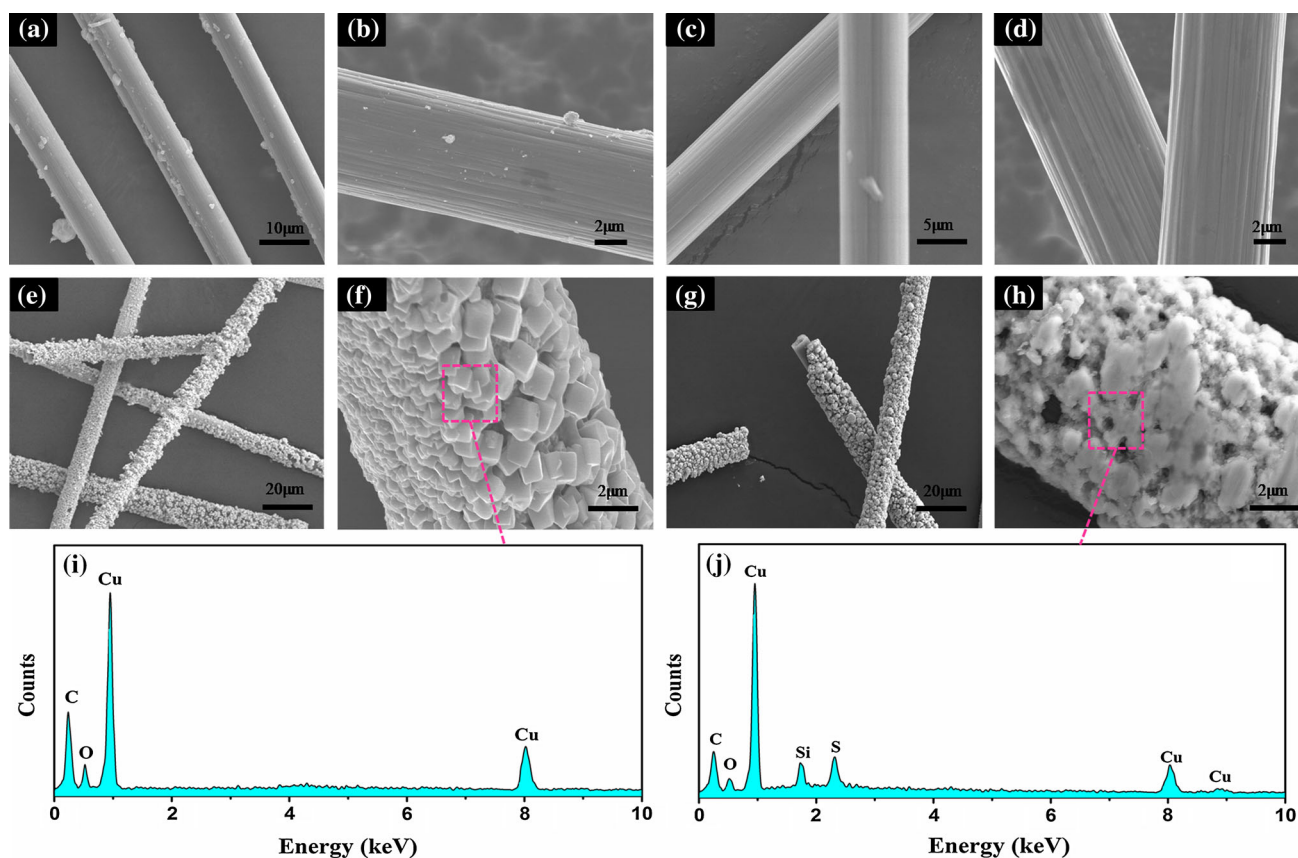


**Fig. 5** SEM images of (a, b) raw-CF, (c, d) Ag-CF, (e, f) Cu-CF, and (g, h) M-Cu-CF, and EDS spectra of (i) Cu-CF and (j) M-Cu-CF

thoroughly and the coating is deposited uniformly on the surface of each fiber. In the higher magnification image, some areas of the copper coating appear like cubes, which agrees well with the consequence of XRD. After coating MPTS, the fibers' surfaces become mellow and the edges and corners vanish, demonstrating the formation of MPTS layer (as shown in Fig. 5g, h). In addition, the EDS results of the fibers (Fig. 5i, j obtained from Fig. 5f, h) reveal the elements existing on the surfaces of the fibers. There is no signal of oxygen detected on the spectrum of Cu-CF, indicating no oxidation of the Cu layer. Besides, the silicon and sulfur signals appear on the spectrum of M-Cu-CF, while these two signals do not exist on that of Cu-CF, further indicating the deposition of the MPTS molecules on Cu-CF.

Figure 6 shows the morphology of the fractured surfaces of different SR composites. To some extent, the dispersion and compatibility of the fillers in the matrix could be reflected by the fractured surfaces. As shown in Fig. 6a, c, e, the fibers can be homogeneously dispersed into SR substrate without aggregation, benefiting uniformly thermal and electrical conduction in the composites. However, Fig. 6b, d reveals the poor compatibility and low adhesion between the fibers and the polymer matrix. Some obvious

gaps are observed, confirming no interactions between the CF, Cu-CF, and polymer matrix, which further influence the enhancement of the thermal and electrical properties of the polymer composites. In the case of M-Cu-CF/SR composites, the M-Cu-CF possesses a relatively good compatibility in the matrix, and no fiber/matrix gaps are discovered on the fracture surface (Fig. 6f), availing the heat conduction between the fibers and the matrix. Furthermore, the contact area of M-Cu-CF and SR matrix is smooth, as directed by the red arrows, and the SR molecules seem to be grafted onto the fibers. This interaction can preferably promote the heat and electricity conduction between the fibers and the polymer matrix efficiently to improve the properties of the composites.

### Thermal properties

The thermal conductivities of composites with various kinds of fillers were measured at a temperature of 25 °C. As can be seen in Fig. 7a, with the addition of filler loadings, the three curves give birth to the same tendency that the thermal conductivities of the polymer composites increase. However, the raw-CF/SR composites exhibit the poorest thermal conductivity of all the composites with the

**Fig. 6** SEM images of **a** and **b** raw-CF/SR composite, **c** and **d** Cu-CF/SR composite, and **e** and **f** M-Cu-CF/SR composite at lower and higher magnifications

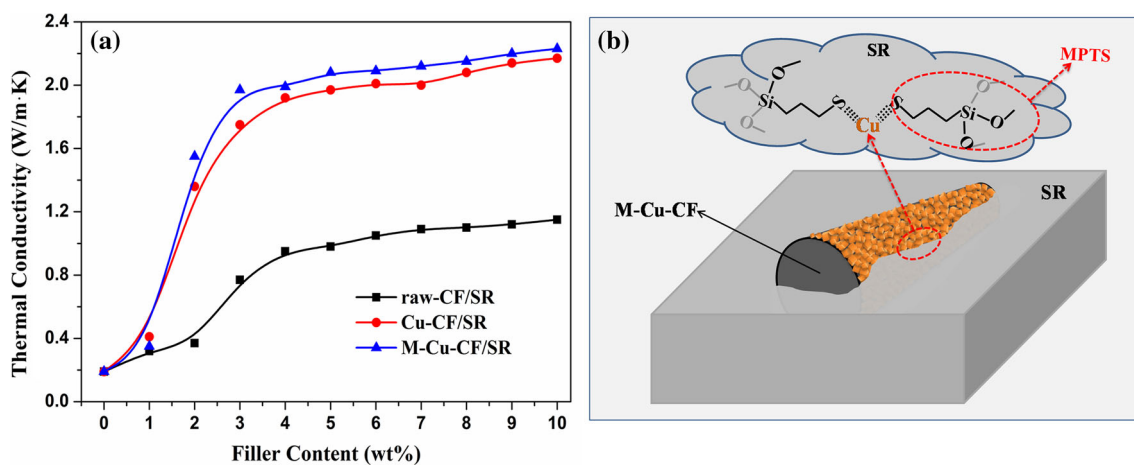
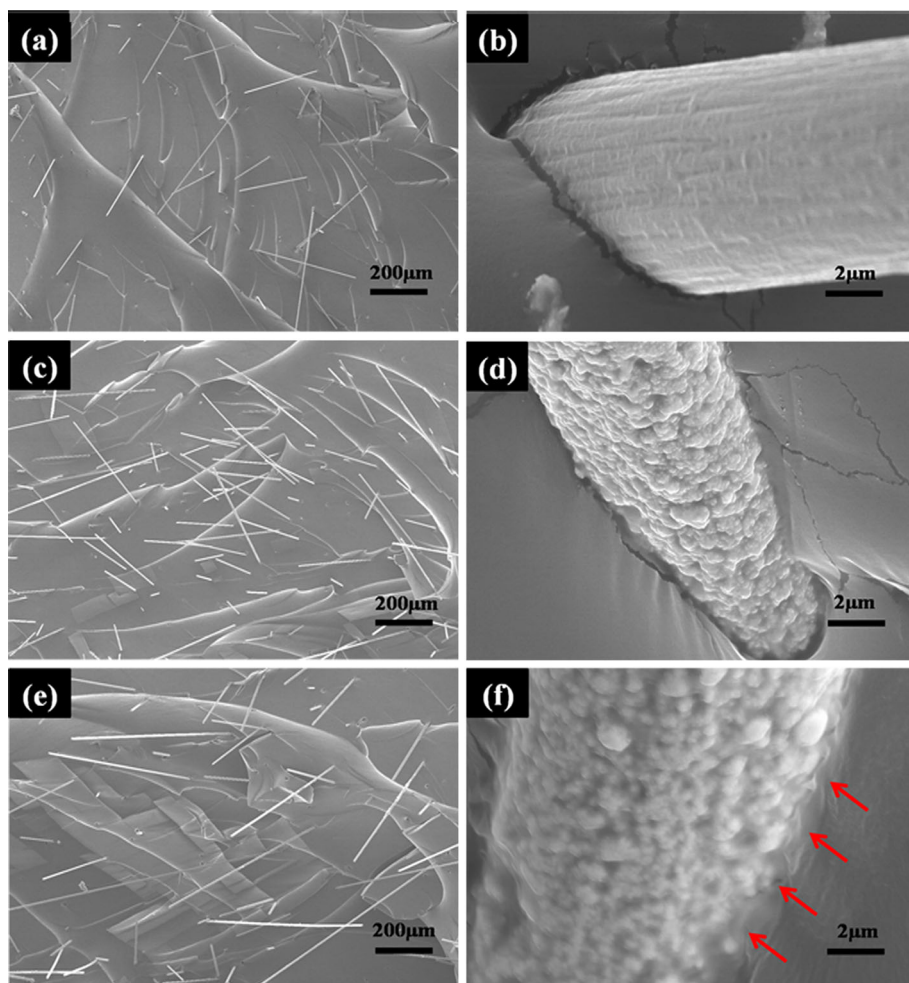


**Fig. 7** **a** Thermal conductivity of raw-CF/SR, Cu-CF/SR, and M-Cu-CF/SR composites, and **b** model structure of M-Cu-CF/SR composite

percolation threshold of the composites of about 1.5 wt% filler content. By contrast, the Cu-CF/SR and M-Cu-CF/SR composites reveal a better thermal conductivity and the percolation threshold is about 0.5 wt% filler content. When

the filler loadings are less than the percolation thresholds, the thermal conductivities of their relative composites increase slowly. This is likely attributable to the large interfacial thermal resistance of the thick layer of polymer

matrix surrounding the fibers. Furthermore, with the filler loadings increasing to about 4.0 wt%, the thermal conductivities of the three kinds of polymer composites increase dramatically due to the gradual formation of a conductive interconnected network, which possesses a lower thermal resistance than the substrate to facilitate heat transmission. Nevertheless, after the filler loadings are more than 4.0 wt%, thanks to the thermal conductive paths tending to be saturated, the thermal conductivities increase slowly again.

The heat conduction in polymer is primarily through phonons and atomic vibration since the free movement of electrons is impossible [31]. The SR substrate, an amorphous polymer, possesses a thermal conductivity of  $0.19 \text{ W (m K)}^{-1}$  due to phonon scattering of crystal defects and atomic vibration along the polymer molecule chains, while Cu owns an excellent heat transportation ability by free electrons with a thermal conductivity of about  $400 \text{ W (m K)}^{-1}$  at room temperature. At the same filler loadings, Cu-CF/SR and M-Cu-CF/SR composites exhibit higher thermal conductivity than raw-CF/SR composites. With the filler loading increasing to 4.0 wt%, the thermal conductivity of raw-CF/SR composites reaches  $0.95 \text{ W (m K)}^{-1}$ , a moderate potentiation. However, at the same loading, M-Cu-CF/SR and Cu-CF/SR composites possess thermal conductivity values of  $1.99 \text{ W (m K)}^{-1}$  and  $1.92 \text{ W (m K)}^{-1}$ , approximately 2.10 times and 2.02 times higher than that of raw-CF/SR composites, respectively. Furthermore, the thermal conductivities of raw-CF/SR, Cu-CF/SR, and M-Cu-CF composites increase to 1.15, 2.17, and  $2.23 \text{ W (m K)}^{-1}$ , respectively, with the filler loadings of up to 10 wt%. Besides, the thermal conductivity of M-Cu-CF/SR composites is always higher than that of Cu-CF/SR almost throughout the process, which means a better compatibility of M-Cu-CF than Cu-CF with the matrix, in accordance with the consequence of SEM. As shown in Fig. 7b, the Cu on the CF could absorb the S of MPTS to form Cu-S, further forming MPTS layer [32]. And the MPTS exhibits a good compatibility with the substrate, boosting the dispersion and improving the interaction of M-Cu-CF with the SR matrix. It is easier for M-Cu-CF than Cu-CF to form a thermal conductive network in the matrix, and the heat conduction between M-Cu-CF and SR substrate is more efficient, so M-Cu-CF have a better reinforcement on thermal conductivity.

### Electrical properties

Figure 8 shows the plots of electrical conductivity versus different loadings of various fillers for SR composites. It can be seen that the electrical conductivities of all the three composites increase with the increasing filler content, which is similar to the tendency of the thermal

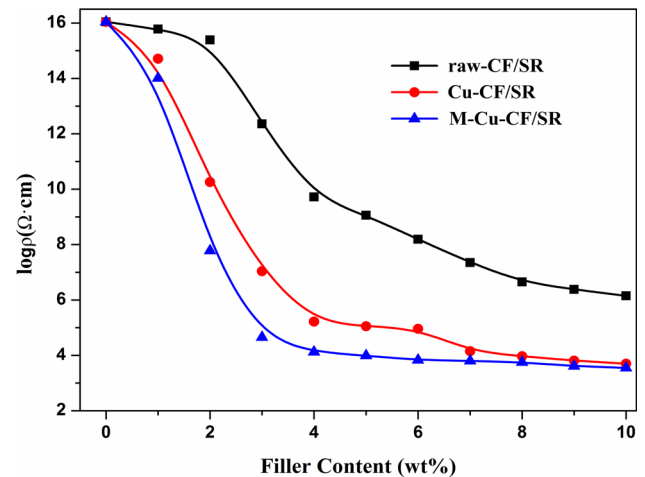


**Fig. 8** Electrical conductivity of raw-CF/SR, Cu-CF/SR, and M-Cu-CF/SR composites

conductivity. The percolation threshold of raw-CF/SR composites is at about the filler content of 2.0 wt%, and the least volume resistivity is about  $1.4 \times 10^6 \Omega \text{ cm}$ . While Cu-CF/SR and M-Cu-CF/SR composites display a better electrical conductivity, and the least volume resistivity is  $5.0 \times 10^3$  and  $3.5 \times 10^3 \Omega \text{ cm}$ , respectively. The percolation thresholds of both Cu-CF/SR and M-Cu-CF/SR composites are about 0.5 wt%, and Cu-CF/SR composites emerge double-percolation phenomenon at 6.0 wt% filler content, which may be due to the further formation of conductive network in the matrix. As we all know, the electrical conduction in the composites mainly depends on the conductive fillers. It is easier for M-Cu-CF to form electrical conductive network with a better compatibility in the SR substrate than Cu-CF. So M-Cu-CF could reach the least volume resistivity with less filler content than Cu-CF, demonstrating a better enhancement function.

### Conclusion

In summary, a thermal and electrical conductive filler was fabricated by chemical plating Cu and MPTS on the surface of CF. The Cu layer was coated on the CF surface without Cu oxide phase detected in XRD and EDS spectrum, and the MPTS layer was verified by the consequences of FTIR and TGA successfully. The M-Cu-CF/SR composites were prepared, and the composites with 4.0 wt% loading had a thermal conductivity of  $1.99 \text{ W (m K)}^{-1}$ , approximately 2.10 times higher than that of raw-CF/SR composites at the same loading. With the increase of M-Cu-CF loading, the least volume resistivity of M-Cu-CF/SR composites is  $3.5 \times 10^3 \Omega \text{ cm}$ . The thermal and electrical conductivities of M-Cu-CF displayed the best enhancement compared to CF and Cu-CF in

SR matrix. We believe that, as a compatible filler, M–Cu–CF can be applied for many other polymer composites to improve the thermal and electrical properties.

**Acknowledgements** This work is supported by the Doctoral Fund of Ministry of Education of China (No. 20121101110014).

**Compliance with ethical standards**

**Conflict of interest** None declared.

## References

- Barba AA, Lamberti G, Amore M, Acier D (2006) Carbon black/silicone rubber blends as absorbing materials to reduce electro magnetic interferences (EMI). *Polym Bull* 57:587–593
- Hong J, Choi HS, Lee KS, Shim SE (2012) Thermal properties of poly(dimethyl siloxane) nanocomposite filled with silicon carbide and multiwall carbon nanotubes. *Polym Int* 61:639–645
- Yang D, Zhang W, Jiang B, Guo Y (2013) Silicone rubber ablative composites improved with zirconium carbide or zirconia. *Compos Part A* 44:70–77
- Doyle BJ, Corbett TJ, Cloonan AJ, Donnell MR, Walsh MT, Vorp DA, McGloughlin TM (2009) Experimental modeling of aortic aneurysms: novel applications of silicone rubbers. *Med Eng Phys* 31:1002–1012
- Patel M, Skinner AR, Maxwell RS (2005) Sensitivity of condensation cured polysiloxane rubbers to sealed and open-to air thermal ageing regimes. *Polym Test* 25:663–668
- Wang JB, Li QY, Wu CF, Xu HY (2014) Thermal conductivity and mechanical properties of carbon black filled silicone rubber. *Polym Polym Compos* 22:393–399
- Norkhairunnisa M, Azizan A, Mariatti M, Ismail H, Sim LC (2012) Thermal stability and electrical behavior of poly-dimethylsiloxane nanocomposites with carbon nanotubes and carbon black fillers. *J Compos Mater* 46:903–910
- Zhou WY, Qi SH, Tu CC, Zhao HZ, Wang CF, Kou JL (2007) Effect of the particle size of Al<sub>2</sub>O<sub>3</sub> on the properties of filled heat-conductive silicone rubber. *J Appl Polym Sci* 104:1312–1318
- Ma WS, Li J, Zhao XS (2013) Improving the thermal and mechanical properties of silicone polymer by incorporating functionalized graphene oxide. *J Mater Sci* 48:5287–5294. doi:10.1007/s10853-013-7320-y
- Zhou WY, Qi SH, Tu CC, Zhao HZ (2007) Novel heat-conductive composite silicone rubber. *J Appl Polym Sci* 104:2478–2483
- Chiu HT, Sukachonmakul T, Wang CH, Wattanakul K, Guo MT, Wang YH (2014) Fabrication and characterization of silicon-based ceramic/aluminum nitride as thermally conductive hybrid filler in silicone rubber composite. *Mater Chem Phys* 147:11–16
- Ismail AM, Mahmoud KR, Salam MH (2015) Electrical conductivity and positron annihilation characteristics of ternary silicone rubber/carbon black/TiB<sub>2</sub> nanocomposites. *Polym Test* 48:37–43
- Mu QH, Feng SY, Diao GZ (2007) Thermal conductivity of silicone rubber filled with ZnO. *Polym Compos* 28:125–130
- Gulgunje PV, Newcomb BA, Gupta K, Chae HG, Tsotsis TK, Kumar S (2015) Low-density and high-modulus carbon fibers from polyacrylonitrile with honeycomb structure. *Carbon* 95:710–714
- Guo H, Huang YD, Meng LH, Liu L, Fan DP, Liu DX (2009) Interface property of carbon fibers/epoxy resin composite improved by hydrogen peroxide in supercritical water. *Mater Lett* 63:1531–1534
- Zhu XD, Zang CG, Jiao QJ (2014) High electrical conductivity of nylon 6 composites obtained with hybrid multiwalled carbon nanotube/carbon fiber fillers. *J Appl Polym Sci* 131:10610–10620
- Hsiao MC, Liao SH, Yen MY, Ma CC, Lee SJ, Chen YH, Huang CH, Lin YF, Xie XF (2010) Electrical and thermal conductivities of novel metal mesh hybrid polymer composite bipolar plates for proton exchange membrane fuel cells. *J Power Sour* 195:509–515
- Xing YJ, Cao W, Li W, Chen HY, Miao W, Wei HX, Hu DM, Chen MH, Li QW (2015) Carbon nanotube/Cu nanowires/epoxy composite mats with improved thermal and electrical conductivity. *J Nanosci Nanotechnol* 15:3265–3270
- Tzeng SS, Chang FY (2001) EMI shielding effectiveness of metal-coated carbon fiber-reinforced ABS composites. *Mater Sci Eng, A* 302:258–267
- Singh BB, Balasubramanian M (2009) Processing and properties of copper-coated carbon fibre reinforced aluminium alloy composites. *J Mater Process Technol* 209:2104–2110
- Zuo JD, Chen SJ, Luo CY, Chen DZ (2015) Preparation of electroless copper coated glass fiber and piezoresistive properties of copper coated glass fiber reinforced plastics. *Appl Surf Sci* 349:319–326
- Yang LW, Liu ZG, Yao GC (2005) The research of depositing copper on carbon fiber. *Mater Sci Technol* 13:620–622
- Omar GV, Raquel LR, Enrique SG, Luis Y, Moya S, Ziolo RF (2014) Graphene oxide modification with graft polymers via nitroxide mediated radical polymerization. *Polymer* 55:2347–2355
- Parambath VB, Nagar R, Sethupathi K, Ramaprabhu S (2011) Investigation of spillover mechanism in palladium decorated hydrogen exfoliated functionalized graphene. *J Phys Chem C* 115:15679–15685
- Ou JF, Wang JQ, Liu S, Mu B, Ren JF, Wang HG, Yang SR (2010) Tribology study of reduced graphene oxide sheets on silicon substrate synthesized via covalent assembly. *Langmuir* 26:15830–15836
- Zhou GH, Yu S, He LL, Guo QG, Ye HQ (2012) The interpretation of X-ray diffraction from the pyrocarbon in carbon/carbon composites with comparison of TEM observations. *Philos Mag* 92:1198–1211
- Yu SG, Park B, Park C, Hong SM, Han TH, Koo CM (2014) RTA-treated carbon fiber/copper core/shell hybrid for thermally conductive composites. *ACS Appl Mater Interfaces* 6:7498–7503
- Kuila T, Khanra P, Mishra AK, Kim NH, Lee JH (2012) Functionalized-graphene/ethylene vinyl acetate co-polymer composites for improved mechanical and thermal properties. *Polym Test* 31:282–289
- Wan YJ, Tang LC, Yan D, Zhao L, Li YB, Wu LB, Jiang JX, Lai GQ (2013) Improved dispersion and interface in the graphene/epoxy composites via a facile surfactant-assisted process. *Compos Sci Technol* 82:60–68
- Che DH, Yao GC, Cao Z (2012) A precious metal-free electroless technique for the deposition of copper on carbon fibers. *Metall Mater Trans A* 43A:4194–4199
- Han ZD, Fina A (2011) Thermal conductivity of carbon nanotubes and their polymer nanocomposites: a review. *Prog Polym Sci* 36:914–944
- Sinapi F, Delhalle J, Mekhalif Z (2002) XPS and electrochemical evaluation of two-dimensional organic films obtained by chemical modification of self-assembled monolayers of (3-mercaptopropyl)trimethoxysilane on copper surfaces. *Mater Sci Eng C* 22:345–353